

Long-distance feedback to cold atoms coupled to an optical nanofiber

M. Sadeghi,* W. Crump, S. Parkins, and M.D. Hoogerland†

*Department of Physics and Dodd-Walls Centre for Photonic and Quantum Technologies,
University of Auckland, Private Bag 92019, Auckland, New Zealand*

We investigate the interaction of spontaneous emission photons generated by a strongly driven laser-cooled atom sample with that same sample after a time delay, which is important for establishing long-distance entanglement between quantum systems. The photons are emitted into an optical nanofiber, connected to a length of conventional optical fiber and reflected back using a Fiber-Bragg Grating mirror. We show that the photon count rates as a function of exciting laser frequency and intensity follow a simple model.

1. INTRODUCTION

The interaction of quantum systems over long distances is a key component of sharing quantum information, leading eventually to distributed quantum computing [1–3]. Quantum information has been shared over long distances using free space or optical fibre distribution of entangled photons [4, 5]. Optical fibre has a distinct advantage of allowing essentially infinitely distant communications [6]. However, the coupling of the state of local quantum systems to photons in an optical fiber has remained a challenge [7, 8].

A promising avenue to address this challenge is using optical nanofibers, which provide robust coupling through the nanofiber’s evanescent field [9, 10]. In many experimental configurations involving atoms around nanofiber, atoms are typically probed with light traveling through the nanofiber. Strong coupling between cold atoms and fiber-ring resonators in such setups has demonstrated clear evidence of vacuum Rabi splitting and non-Markovian behavior [11, 12]. We utilize a perpendicular side-probe laser to excite the atoms around the nanofiber, allowing their spontaneously emitted photons to couple into the nanofiber’s mode.

The spontaneous emission rate and its characteristics, including frequency, intensity, polarization, and direction, are influenced by the photon density of states and vacuum field fluctuations [13–15], especially in environments like cavities, waveguides, half-cavities, and photonic crystals [16–18]. Studies have shown how these environments modify spontaneous emission rates and atomic energy levels, with effects observed in many experimental setups [12, 19–22]. Additionally, the use of optical nanofiber (ONF) in spontaneous emission studies reveals that the evanescent field and van der Waals surface interactions can significantly alter the spontaneous emission properties of atoms [23–25].

When a feedback mirror is positioned at a far distance from the emitter, such that it introduces a time delay much longer than the emitter’s natural decay time, feedback photons can be reabsorbed after the atom has re-

turned to its ground state. In this case, the reflected light does not interfere with the original outgoing emission; it is re-emitted, resulting in successive spikes in the emission rate over time [26, 27]. However, when the feedback mirror creates a delay that is comparable to the emitter’s lifetime, interference effects may emerge, and the phase of the reflected light relative to the emitted light can play an important role, enhancing or diminishing the emission depending on the relative phase [26].

The collective radiative dynamics of quantum emitters, especially when separated by macroscopic distances, can show non-Markovian features. In such cases, the system’s evolution is influenced by time-delayed feedback from the electromagnetic field, leading to modified spontaneous emission rates for superradiant and subradiant states [28]. Pichler et al. [29] propose a protocol to generate complex entangled photonic states using a single quantum emitter and time-delayed quantum feedback. The photons emitted from the quantum emitter can interact with the emitter multiple times due to feedback, creating correlations between them and transforming a 1D entangled state into a 2D cluster state.

In this paper, we report on long-distance interactions between cold neutral atoms and a distant mirror, mediated by an optical nanofiber and regular optical fiber. This interaction is driven by photons emitted from excited atoms into the nanofiber, which are then reflected by a distant fiber-Bragg grating (FBG) mirror, creating a feedback that modifies the emission properties of the system. As the photon’s travel time to the FBG is much longer than the spontaneous lifetime of the atoms, effects of sub- or super-radiance are suppressed. This is the most likely scenario in real-world long-distance interactions between quantum systems. Here, we present our results on how feedback-induced reabsorption leads to spectral broadening and frequency shifts in the emission spectrum.

2. EXPERIMENTAL CONFIGURATION

The diagram in Fig. 1 presents a schematic of the experimental setup used in this study. A Magneto-Optical Trap (MOT) [30, 31] creates a cold cloud of approximately 5 million atoms at a temperature of around

* msad106@aucklanduni.ac.nz

† m.hoogerland@auckland.ac.nz

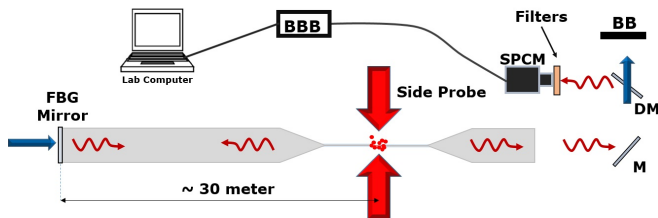


FIG. 1. Schematic of the experimental setup. The FBG is approximately 30 meters away from the atoms, with a reflectance of 97%. The components are filters, a beam blocker (BB), a single-photon counting module (SPCM), a Beaglebone black (BBB), a mirror (M), and a dichroic mirror (DM). The probe polarization is perpendicular to the nanofiber waist.

150 μK surrounding the waist of an ONF, which has a diameter of approximately 380 nm. At typical MOT densities, in our experimental setup, we estimate fewer than ten atoms within the evanescent field of the ONF. The MOT setup is similar to the one used in Ref. [11].

The ONF was fabricated in-house using the flame-brush technique, starting from standard single-mode optical fiber. During fabrication, the fiber is simultaneously heated and stretched, creating an adiabatic transition between the standard and stretched portions of the fiber [31–33]. The ONF is single mode at the D_2 resonant wavelength of 852 nm and is placed inside an ultra-high vacuum chamber. At the center of the chamber, the waist of the ONF intersects with the cloud of cold cesium atoms produced by the MOT. The cesium cloud is loaded from a background gas generated by a ^{133}Cs dispenser.

Atoms very close to the ONF adhere to its surface due to van der Waals forces [25], resulting in a cesium coating that forms after approximately one minute of exposure. This coating reduces light transmission to less than 40%. To address this issue, a 685-nm laser beam with a power of around 0.4 mW is employed during the MOT-on stage, which effectively keeps atoms away from the nanofiber surface. When the MOT beams are turned off, the repulsive laser beam is also deactivated, allowing the atoms to approach the nanofiber for probing.

The atoms are excited using probe pulses nearly resonant with the $F = 4 \rightarrow F' = 5$ transition of the ^{133}Cs D_2 line. The exciting beam’s power and frequency are controlled by an Acousto-Optic Modulator in a double-pass configuration. The beam is coupled into a polarization-maintaining, single-mode fiber. The fiber’s output forms a side excitation beam that propagates perpendicularly to the ONF waist in a standing wave configuration. The standing wave arrangement minimizes the momentum transfer from the exciting laser to atoms, which is achieved by directing the reflected beam back toward its source. The collimated side probe beam has a $1/e^2$ full width of approximately 1.5 mm.

The radio-frequency signal to drive the Acousto-Optic Modulator is derived from a digital signal generator around 80 MHz. The radio-frequency amplitude is con-

trolled by an Arbitrary Function Generator (Tektronix 3032) via an RF switch. A train of 150 ns long pulses, repeated every 600 ns, was programmed into the Function Generator and triggered by the experiment computer for each experiment.

Spontaneous emission photons are emitted into the nanofiber in both directions with each exciting laser pulse. Photons traveling in one direction propagate along a short length of single-mode fiber to the Single Photon Counting Module (Perkin-Elmer SPCM-AQRH-3X-W3). Photons emitted in the opposite direction travel through a longer length of single-mode fiber to an FBG, where they are reflected. After the round trip, these reflected photons interact with the atomic sample. By this time, the excitation laser has turned off, and the atoms have returned to their ground state. Following this interaction, the photons—already attenuated by both fiber losses and re-absorption by the atoms—also propagate to the SPCM for detection.

The SPCM output pulses are time-tagged by the Programmable Realtime Unit on a BeagleBone minicomputer with a time resolution of 5 ns. The arrival times of all photons from one experiment run, consisting of 2000 exciting laser pulses, are transferred to the laboratory computer.

For each experiment, the MOT is filled with atoms at a MOT laser detuning of 12 MHz. The MOT lasers are then switched to a detuning of 10 MHz for additional cooling for 0.5 ms. Subsequently, the MOT lasers are extinguished, and the excitation laser pulse train is triggered. In Fig. 2, we show histograms of the arrival times of photons on the detector. The experiment is run 120 times for each detuning and excitation power.

As the exciting probe laser is heating the atoms in the cloud, we found that the count rate diminishes after a number of excitation pulses, depending on the probe laser intensity and detuning. Therefore, we have chosen to limit the number of detected photons to 1500 for each atom cloud in post-processing, as the number of photons detected is a good indicator of the degree of heating in the cloud. Given the time when the last photon is detected, we establish a count rate.

3. EXPERIMENTAL RESULTS

In this section, we present the main results of our experiment, focusing on the spontaneously emitted photons of cold cesium atoms coupled to an ONF for various excitation intensities and detunings, and considering the influence of long-time delayed feedback on the emitted spectra. The first set of results examines the saturation behavior of the system, followed by an exploration of the role of the Mollow spectrum in the system and frequency shifts arising from surface and feedback interactions.

Fig. 3 presents the count rate as a function of the laser intensity for on-resonance excitation. We scale the intensity such that half of the maximum count rate for the

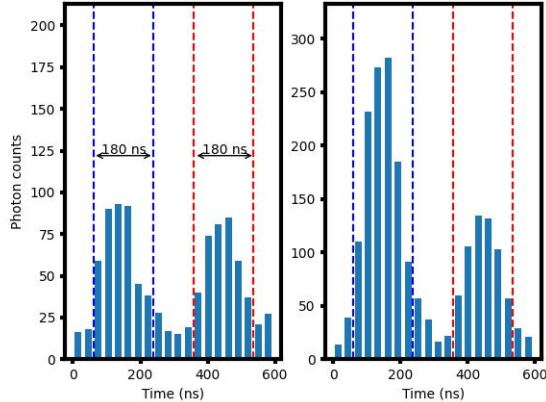


FIG. 2. Photon arrival histogram for an excitation laser power of $40 \mu\text{W}$, which corresponds to $s_0 = I/I_0 = 0.4$, for two values of the laser detuning: $\Delta = 30 \text{ MHz}$ (left) and $\Delta = 0 \text{ MHz}$ (right). The first peak represents photons that have been emitted into the ONF towards the detector. The second peak represents photons that have been emitted towards the FBG, reflected, interacted with the ground state atoms in the MOT before being detected. In the data analysis, photon counts from emission and feedback photons were considered within the 180 ns time interval indicated by the horizontal arrows.

direct fluorescence is reached at $s_0 = 1$, according to the well-known scaling for the excited state population n_e in a two-level system,

$$n_e = \frac{s_0}{2(1 + s_0)}, \quad (1)$$

where $s_0 = I/I_0$, I is the laser intensity, and I_0 is the saturation intensity. This scaling yields a saturation power of $121 \mu\text{W}$, which agrees with our estimates of the laser beam size. The blue curve in the graph corresponds to Eq. (1). In the inset of Fig. 3, we show the ratio of the indirect and direct fluorescence rate. The relative amount of absorption reduces as the exciting laser power is increased. The atoms around the nanofiber are excited by a laser beam that may exceed the saturation intensity. As a result, the emission into the fiber follows a frequency spectrum characteristic of the Mollow spectrum [34–36]. This fluorescence spectrum can be expressed as

$$g_{sc}(\omega) = \frac{s}{(2+s)^2} \delta(\omega) + \frac{s_0}{8\pi\Gamma} \frac{s}{1+s} \times \frac{1 + s_0/4 + (\omega/\Gamma)^2}{\left[\frac{1}{4} + \frac{s_0}{4} + \left(\frac{\Delta}{\Gamma}\right)^2 - 2\left(\frac{\omega}{\Gamma}\right)^2\right]^2 + \left(\frac{\omega}{\Gamma}\right) \left[\frac{5}{4} + \frac{s_0}{2} + \left(\frac{\Delta}{\Gamma}\right)^2 - \left(\frac{\omega}{\Gamma}\right)^2\right]^2} \quad (2)$$

where the first term represents elastic scattering at the frequency of scattered photons relative to laser frequency, ω , and the second term is inelastic scattering with Δ the laser detuning and Γ the natural decay rate. The ratio of the inelastic and elastic scattering power comes out as the frequency-dependent saturation parameter s , defined by

$$s(\Delta) = \frac{s_0}{1 + 4(\Delta/\Gamma)^2}. \quad (3)$$

All photons emitted into the nanofiber, both towards the detector and towards the FBG mirror, are assumed to be described by this spectrum.

To obtain the fitted curve for the indirect fluorescence in Fig. 3 (red curve), we take the Mollow spectrum, given by Eq. (2) for the intensities obtained above. Light with this spectrum then interacts with the ground state atoms in the MOT. Our data shows that, on average, fewer than one photon is emitted per excitation laser pulse, resulting in a very low intensity of the fluorescence photons. The light is attenuated according to a Lorentzian spectrum as described by the Beer-Lambert law,

$$I = I_0 e^{-\alpha L}, \quad (4)$$

where I_0 is the intensity of reflected photons from the FBG mirror, α is the optical depth, and L represents the frequency-dependent Lorentzian absorption profile. Using the width and depth of this absorption spectrum as parameters, we obtain a best fit for a width of $(6.7 \pm 0.6) \text{ MHz}$ and an optical depth of (0.85 ± 0.04) . Note that the changing ratio of count rates is well reproduced by this model for higher excitation laser powers. Intuitively, we interpret these results as displaying that at higher excitation laser powers the Mollow sidebands are out of resonance with the atoms and are not absorbed.

In a further experiment, we vary the detuning of the excitation laser and record the count rates, as presented in Fig. 4(a). It should be noted that the width of the fitted Lorentzian curve for the direct excitation spectrum is 16 MHz , much larger than the natural linewidth of the transition, which is 5.2 MHz . However, this is similar to results from other groups [37] and we attribute this larger linewidth to a combination of surface interactions, magnetic field gradients, and laser linewidth.

Finally, we take the ratio of indirect and direct photon flux and plot this as a function of detuning, as shown in Figs. 4(b,d). This represents an absorption spectrum for

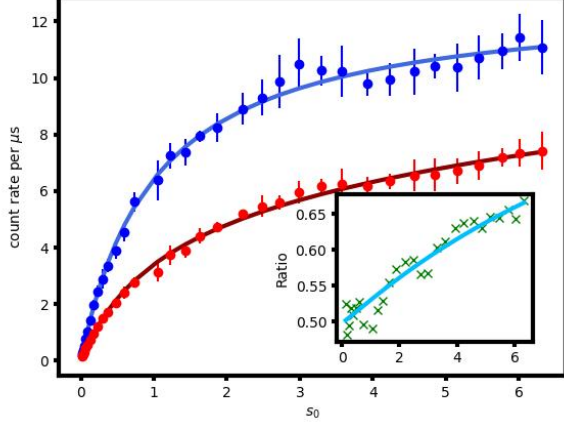


FIG. 3. The photon count rate for the direct (blue dots) and indirect (red dots) fluorescence as a function of the saturation parameter s_0 . In the inset, the ratio of the count rates is shown. The laser detuning $\Delta = 0$. The points represent the mean photon count rates and error bars show the standard deviation across four separate experimental runs.

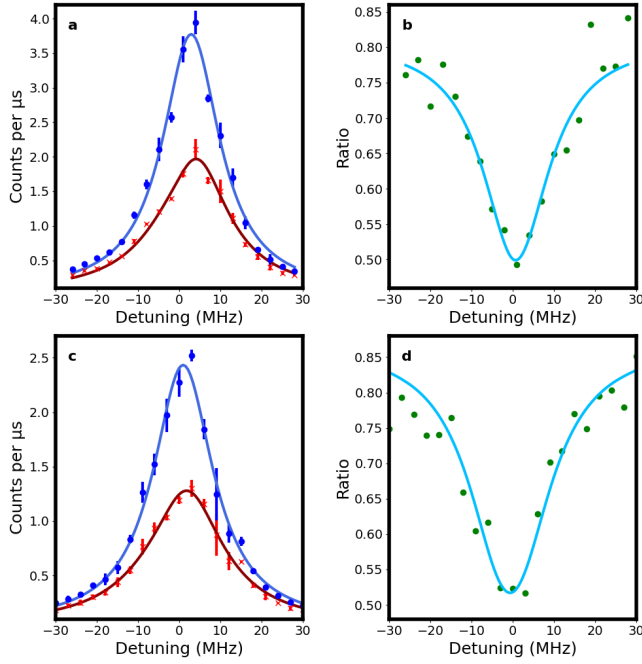


FIG. 4. (a, c) The photon count rate for direct fluorescence (blue dots) and indirect fluorescence (red crosses) as a function of detuning for excitation powers of (a) $40 \mu\text{W}$ and (c) $150 \mu\text{W}$, corresponding to saturation parameters $s_0 = I/I_0 = 0.4$ and $s_0 = 1.2$, respectively. The points represent the mean values, and the error bars show the standard deviation from three different experimental runs. The blue line for the direct fluorescence is a Lorentzian fit. (b, d) The ratio of indirect to direct fluorescence as a function of detuning. The indirect fluorescence and the ratio are modeled as described in the text.

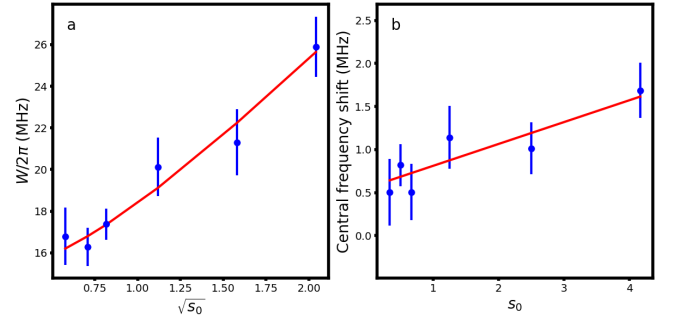


FIG. 5. (a) The direct fluorescence linewidth as a function of the square root of the saturation parameter, showing an increase in linewidth with excitation power. The total linewidth is the sum of the natural linewidth and additional broadening. (b) The central frequency shift between direct and indirect fluorescence as a function of excitation power. The shift increases with the excitation power, and the error bars indicate uncertainties.

the spontaneously emitted photons.

We then model the indirect fluorescence photons as follows: (1) For each excitation laser detuning Δ , the number of photon emissions towards the FBG is the same as the number emitted directly towards the detector, $n_p(\Delta)$. (2) The spectrum of the emitted photons is given by Eq. (2), but normalised to unity. (3) After reflecting off the FBG mirror, these photons may be reabsorbed by the atoms, following the Beer-Lambert law and a Lorentzian absorption profile, with a width given by the width of the emission spectrum at low power but with a frequency shift as a free parameter. The fitted curves in Figs. 4(b,d) are from the ratio of the fitted curves in Fig. 4(a,c).

The linewidth of the direct fluorescence is expected to increase with the Rabi frequency of the atoms in the excitation beam. To verify this assumption, we again take excitation spectra, showing the number of photons emitted directly towards the SPCM as a function of the detuning of the excitation laser, but for a range of intensities. In Fig. 5(a), the linewidth of the direct fluorescence is plotted against the square root of the saturation parameter. The plot shows that the linewidth increases with power, reflecting the broadening effect as the system is driven into the stronger coupling regime. The fitted curve represents the linewidth described by the equation:

$$W(s_0) = \Gamma\sqrt{s_0 + 1} + \Gamma_0, \quad (5)$$

where Γ is the natural atomic decay rate and Γ_0 accounts for additional broadening due to surface interactions, magnetic field gradients, and laser linewidth. From the fitting, we obtain $\Gamma = (6.45 \pm 1.17) \text{ MHz}$ and $\Gamma_0 = (8.44 \pm 0.80) \text{ MHz}$, indicating a significant contribution to the linewidth beyond the natural decay rate.

In Figs. 4(c,d), at higher excitation laser powers, we observe a small shift in the spectrum of the direct fluorescence relative to the indirect fluorescence. This frequency shift is limited to a few MHz, i.e., less than the natural

linewidth of the transition. In Fig. 5(b), the frequency shift between direct and indirect fluorescence is plotted as a function of excitation power, indicating that the frequency shift increases with intensity. The slope of this fit is approximately (0.25 ± 0.06) MHz, which may reflect the increasing influence of surface interactions as the system is driven more strongly. That is, the shift could be explained by an effect where atoms for which the resonance frequency is shifted due to surface interactions may also be excited by the laser at higher intensities.

4. CONCLUSION AND OUTLOOK

In this study, we examined the spontaneous emission of cold, driven cesium atoms coupled to an optical nanofiber and the effects of long-delay feedback on this emission. The results show that the fluorescence spectrum broad-

ens as the excitation intensity increases. When the spontaneously emitted photons, reflected by a FBG mirror, return to interact with the atoms in their ground state, reabsorption occurs, a behavior effectively modeled using the Mollow spectrum to describe the original emission. We also observe a shift in frequency between direct and indirect fluorescence, with the shift increasing at higher intensities.

The reabsorption effects for atoms in front of a mirror configuration could be further explored by increasing the interaction times. We aim to achieve this by trapping the atoms on the nanofiber using a two-color dipole trap [38]. Furthermore, we aim to improve the switching time of the exciting laser to times shorter than the spontaneous emission lifetime of the atom, thereby allowing studies of coherent effects such as sub- and super-radiance. These effects of time-delayed feedback may have implications for developing quantum communication networks.

-
- [1] H. J. Kimble, The quantum internet, *Nature* **453**, 1023 (2008).
- [2] A. S. Cacciapuoti, M. Caleffi, F. Tafuri, F. S. Cataliotti, S. Gherardini, and G. Bianchi, Quantum internet: networking challenges in distributed quantum computing, *IEEE Network* **34**, 137 (2019).
- [3] K. Azuma, S. E. Economou, D. Elkouss, P. Hilaire, L. Jiang, H.-K. Lo, and I. Tzitrin, Quantum repeaters: From quantum networks to the quantum internet, *Reviews of Modern Physics* **95**, 045006 (2023).
- [4] J.-W. Pan, C. Simon, Č. Brukner, and A. Zeilinger, Entanglement purification for quantum communication, *Nature* **410**, 1067 (2001).
- [5] N. Gisin and R. Thew, Quantum communication, *Nature Photonics* **1**, 165 (2007).
- [6] L.-M. Duan, M. D. Lukin, J. I. Cirac, and P. Zoller, Long-distance quantum communication with atomic ensembles and linear optics, *Nature* **414**, 413 (2001).
- [7] K. Hammerer, A. S. Sørensen, and E. S. Polzik, Quantum interface between light and atomic ensembles, *Reviews of Modern Physics* **82**, 1041 (2010).
- [8] A. Reiserer and G. Rempe, Cavity-based quantum networks with single atoms and optical photons, *Reviews of Modern Physics* **87**, 1379 (2015).
- [9] E. Vetsch, *Optical interface based on a nanofiber atom-trap*, Ph.D. thesis, University of Mainz (2010).
- [10] A. Goban, *Strong atom-light interactions along nanostructures: Transition from free-space to nanophotonic interfaces*, Ph.D. thesis, California Institute of Technology (2015).
- [11] S. K. Ruddell, K. E. Webb, I. Herrera, A. S. Parkins, and M. D. Hoogerland, Collective strong coupling of cold atoms to an all-fiber ring cavity, *Optica* **4**, 576 (2017).
- [12] D. Lechner, R. Pennetta, M. Blaha, P. Schneeweiss, A. Rauschenbeutel, and J. Volz, Light-matter interaction at the transition between cavity and waveguide QED, preprint arXiv:2302.07161 (2023).
- [13] A. Ferreri, M. Domina, L. Rizzuto, and R. Passante, Spontaneous emission of an atom near an oscillating mirror, *Symmetry* **11**, 1384 (2019).
- [14] K. P. Nayak, P. N. Melentiev, M. Morinaga, F. Le Kien, V. I. Balykin, and K. Hakuta, Optical nanofiber as an efficient tool for manipulating and probing atomic fluorescence, *Optics Express* **15**, 5431 (2007).
- [15] F. Le Kien, S. D. Gupta, V. Balykin, and K. Hakuta, Spontaneous emission of a cesium atom near a nanofiber: Efficient coupling of light to guided modes, *Physical Review A* **72**, 032509 (2005).
- [16] E. M. Purcell, Spontaneous emission probabilities at radio frequencies, *Physical Review* **69**, 674 (1946).
- [17] P. Lodahl, S. Mahmoodian, and S. Stobbe, Interfacing single photons and single quantum dots with photonic nanostructures, *Reviews of Modern Physics* **87**, 347 (2015).
- [18] D. Kleppner, Inhibited spontaneous emission, *Physical Review Letters* **47**, 233 (1981).
- [19] J. Eschner, C. Raab, F. Schmidt-Kaler, and R. Blatt, Light interference from single atoms and their mirror images, *Nature* **413**, 495 (2001).
- [20] P. Goy, J. M. Raimond, M. Gross, and S. Haroche, Observation of cavity-enhanced single-atom spontaneous emission, *Physical Review Letters* **50**, 1903 (1983).
- [21] S. Noda, M. Fujita, and T. Asano, Spontaneous-emission control by photonic crystals and nanocavities, *Nature Photonics* **1**, 449 (2007).
- [22] K. H. Drexhage, Interaction of light with monomolecular dye lasers, in *Progress in Optics* (E. Wolfe, Ed., North Holland Publishing) (1974).
- [23] P. Solano, P. Barberis-Blostein, F. K. Fatemi, L. A. Orozco, and S. L. Rolston, Super-radiance reveals infinite-range dipole interactions through a nanofiber, *Nature Communications* **8**, 1857 (2017).
- [24] P. Solano, J. A. Grover, Y. Xu, P. Barberis-Blostein, J. N. Munday, L. A. Orozco, W. D. Phillips, and S. L. Rolston, Alignment-dependent decay rate of an atomic dipole near an optical nanofiber, *Physical Review A* **99**, 013822 (2019).
- [25] B. Patterson, P. Solano, P. Julienne, L. Orozco, and S. Rolston, Spectral asymmetry of atoms in the van der Waals potential of an optical nanofiber, *Physical Review*

- A **97**, 032509 (2018).
- [26] T. Tufarelli, M. Kim, and F. Ciccarello, Non-markovianity of a quantum emitter in front of a mirror, *Physical Review A* **90**, 012113 (2014).
- [27] U. Dorner and P. Zoller, Laser-driven atoms in half-cavities, *Physical Review A* **66**, 023816 (2002).
- [28] K. Sinha, P. Meystre, E. A. Goldschmidt, F. K. Fatemi, S. L. Rolston, and P. Solano, Non-markovian collective emission from macroscopically separated emitters, *Physical Review Letters* **124**, 043603 (2020).
- [29] H. Pichler, S. Choi, P. Zoller, and M. D. Lukin, Universal photonic quantum computation via time-delayed feedback, *Proceedings of the National Academy of Sciences* **114**, 11362 (2017).
- [30] S. Chu, Laser manipulation of atoms and particles, *Science* **253**, 861 (1991).
- [31] S. Ruddell, *Calorimetry of an ultracold Bose gas and cavity quantum electrodynamics with an optical nanofibre*, Ph.D. thesis, University of Auckland (2017).
- [32] T. A. Birks and Y. W. Li, The shape of fiber tapers, *Journal of lightwave technology* **10**, 432 (1992).
- [33] R. Nagai and T. Aoki, Ultra-low-loss tapered optical fibers with minimal lengths, *Optics express* **22**, 28427 (2014).
- [34] B. R. Mollow, Power spectrum of light scattered by two-level systems, *Physical Review* **188** (1969).
- [35] L. Ortiz-Gutiérrez, R. C. Teixeira, A. Eloy, D. F. da Silva, R. Kaiser, R. Bachelard, and M. Fouché, Mollow triplet in cold atoms, *New Journal of Physics* **21**, 093019 (2019).
- [36] M. Das, A. Shirasaki, K. Nayak, M. Morinaga, F. Le Kien, and K. Hakuta, Measurement of fluorescence emission spectrum of few strongly driven atoms using an optical nanofiber, *Optics Express* **18**, 17154 (2010).
- [37] K. Nayak, M. Das, F. Le Kien, and K. Hakuta, Spectroscopy of near-surface atoms using an optical nanofiber, *Optics Communications* **285**, 4698 (2012).
- [38] A. Goban, K. Choi, D. Alton, D. Ding, C. Lacroûte, M. Pototschnig, T. Thiele, N. Stern, and H. Kimble, Demonstration of a state-insensitive, compensated nanofiber trap, *Physical Review Letters* **109**, 033603 (2012).